The crystal structure of paramagnetic copper(ii) oxalate (CuC_2O_4):
formation and thermal decomposition of randomly stacked anisotropic nano-sized crystallites

Christensen, Axel Nørlund; Lebech, Bente; Andersen, Niels Hessel; Grivel, Jean-Claude

Published in:
Dalton Transactions

Link to article, DOI:
10.1039/c4dt01689k

Publication date:
2014

Document Version
Publisher's PDF, also known as Version of record

Dalton Transactions

PAPER

Cite this: *Dalton Trans.*, 2014, **43**, 16754

The crystal structure of paramagnetic copper(II) oxalate (CuC_2O_4): formation and thermal decomposition of randomly stacked anisotropic nano-sized crystallites

Axel Nørlund Christensen,[a] Bente Lebech,*[b,c] Niels Hessel Andersen[c] and Jean-Claude Grivel[d]

Synthetic copper(II) oxalate, CuC_2O_4, was obtained in a precipitation reaction between a copper(II) solution and an aqueous solution of oxalic acid. The product was identified from its conventional X-ray powder patterns which match that of the copper mineral Moolooite reported to have the composition $CuC_2O_4{\cdot}0.44H_2O$. Time resolved *in situ* investigations of the thermal decomposition of copper(II) oxalate using synchrotron X-ray powder diffraction showed that in air the compound converts to Cu_2O at 215 °C and oxidizes to CuO at 345 °C. Thermo gravimetric analysis performed in an inert Ar-gas reveals that the material contains no crystal water and reduces to pure Cu at 295 °C. Magnetic susceptibility measurements in the temperature range from 2 K to 300 K show intriguing paramagnetic behaviour with no sign of magnetic order down to 2 K. A crystal structure investigation is made based on powder diffraction data using one neutron diffraction pattern obtained at 5 K (λ = 1.5949(1) Å) combined with one conventional and two synchrotron X-ray diffraction patterns obtained at ambient temperature using λ = 1.54056, 1.0981 and λ = 0.50483(1) Å, respectively. Based on the X-ray synchrotron data the resulting crystal structure is described in the monoclinic space group $P2_1/c$ (#14) in the $P12_1/n1$ setting with unit cell parameters a = 5.9598(1) Å, b = 5.6089(1) Å, c = 5.1138 (1) Å, β = 115.320(1)°. The composition is CuC_2O_4 with atomic coordinates determined by FullProf refinement of the neutron diffraction data. The crystal structure consists of a random stacking of CuC_2O_4 micro-crystallites where half the Cu-atoms are placed at (2a) and the other half at (2b) positions with the corresponding oxalate molecules centred around the corresponding (2b) and (2a) site positions, respectively. The diffraction patterns obtained for both kinds of radiation show considerable broadening of several Bragg peaks caused by highly anisotropic microstructural size and strain effects. In contrast to the water reported to be present in Moolooite, neither thermogravimetric nor the *in situ* thermal decomposition investigations and crystal structure analysis of the neutron diffraction data revealed any trace of water. An appendix contains details about the profile parameters for the diffractometers used at the European Synchrotron Radiation Facility and the Institute Max von Laue–Paul Langevin.

Received 7th June 2014,
Accepted 9th September 2014

DOI: 10.1039/c4dt01689k

www.rsc.org/dalton

1. Introduction

Oxalic acids and oxalate salts are found in a number of plants, and oxalate found in minerals may be of biological origin. The oxalate minerals Whewellite ($CaC_2O_4{\cdot}H_2O$[1]), Natroxalate ($Na_2C_2O_4$ [2]), and Moolooite[3,4] are such examples. Moolooite is a naturally occurring hydrated copper oxalate from Mooloo Downs in Western Australia apparently formed by interaction of solutions derived from bird guano (the biological source) and weathering copper sulphides.[3] It has also been found together with Whewellite on copper tolerant lichens (the biological source) growing on copper bearing rocks.[4] The crystal structures of the first two mentioned minerals are well established from single crystal X-ray analysis. No single crystal structure analysis has been made on natural Moolooite, but a microchemical analysis indicates the composition $CuC_2O_4{\cdot}0.44H_2O$,[3] and a disordered structure with orthorhombic symmetry and a = 5.35, b = 5.63, c = 2.56 Å and Z = 1 were suggested from powder X-ray patterns.[3] The X-ray powder patterns of natural Moolooite[4] match the reference pattern of

[a]*Crystal Chemistry, Højkolvej 7, DK-8210 Århus V, Denmark*
[b]*Niels Bohr Institute, University of Copenhagen, DK-2100 Copenhagen, Denmark. E-mail: bele@fysik.dtu.dk*
[c]*Department of Physics, Technical University of Denmark, DK-2800 Kgs. Lyngby, Denmark*
[d]*Department of Energy Conversion and Storage, Technical University of Denmark, DK-4000 Roskilde, Denmark*

synthetic copper oxalate hydrate (JCPDS card no. 21-297) and the pattern of $CuC_2O_4{\cdot}0.44H_2O$.[3] A synthetic hydrated copper oxalate was not as well crystallised as the mineral, but had similar cell dimensions a = 5.42(1), b = 5.58(1), c = 2.557(2) Å.[4]

Synthetic copper(II) oxalate[5–7] has been obtained by several authors in a precipitation reaction between a copper nitrate solution and a sodium oxalate solution as nano-sized crystallites, which in contact with the mother liquid grows to a 50–70 nm length over a few weeks.[5] The dry compound transforms by calcination to nano-sized particles of copper when the calcination is performed in a vacuum or in an inert atmosphere.[6,7] The process can be used to prepare copper nanowires.[8] When copper oxalate is calcined in air or in oxygen, the final product is CuO.[6]

Crystal structure analysis on synthetic copper oxalate hydrate $CuC_2O_4{\cdot}xH_2O$ using X-ray powder diffraction has also been reported.[9,10] The hydrated $CuC_2O_4{\cdot}xH_2O$ was established with x = 0.1 and x = 0.4 and a water free sample was obtained when a sample of $CuC_2O_4{\cdot}xH_2O$ was heated in hydrogen to 235 °C.[9] Hydrated synthetic copper(II) oxalate has a powder pattern agreeing with the orthorhombic space group *Pnnm* and cell parameters a = 5.407, b = 5.569, c = 2.546 Å for $CuC_2O_4{\cdot}0.1H_2O$.[9] This corresponds to a cell volume of 76.7 Å^3, which is too small a volume to contain the two formula units required in the *Pnnm* space group. Hence, a monoclinic unit cell with the space group $P2_1/c$ (#14) and unit cell parameters a = 5.098(3), b = 5.376(3), c = 6.159(3) Å, β = 114.45(5)° and Z = 2 was later suggested by the same author.[10] No refinements of crystal structures using this cell has been published. Another monoclinic unit cell with a crystal structure similar to that of β-ZnC_2O_4 (a = 6.158, b = 5.377, c = 5.102 Å, β = 114.5°, Z = 2) and the space group $P2_1/c$ (#14) in the $P12_1/n1$ setting has also been suggested.[11] Based on EXAFS data,[12] a model to deduce the structure of hydrated copper(II) oxalate was suggested.[12,13] In this model a planar $Cu(C_2O_4)Cu$ complex forming infinite ribbons is packed into the structure in an ordered way. Until now, this model has not been confirmed by any structural model refinement of diffraction data.

In view of these inconclusive studies, a crystal structure analysis using neutron- and X-ray diffraction data on synthetic copper(II) oxalate is reported in the following. The results of the analysis are based on accurate neutron and synchrotron X-ray diffraction data supplemented by time resolved studies of the thermal decomposition of copper(II) oxalate, thermogravimetric analysis and measurement of the magnetic susceptibility.

2. Sample preparation

To a boiling solution made of 3.5 g $Cu(NO_3)_2{\cdot}3H_2O$ (Merck) and 100 mL of water was added dropwise a solution made of 1.5 g oxalic acid (Ferak) in 100 mL of water. The precipitate was then washed, filtered and dried at room temperature (sample 1). When the precipitation was done at room temperature, the crystals of copper(II) oxalate were of nano-size, and it was difficult to filter the product. X-ray powder patterns of the prepared samples were recorded on a Stoe–Stadi diffractometer using Cu-Kα1 radiation λ = 1.54056 Å, and 2θ range 5.00 to 89.98° in steps of 0.02°. The final product was identified as $CuC_2O_4{\cdot}xH_2O$ from these patterns (JCPDS card no. 21-297). As an example, the powder diffraction pattern of sample 1 is shown in Fig. 1.

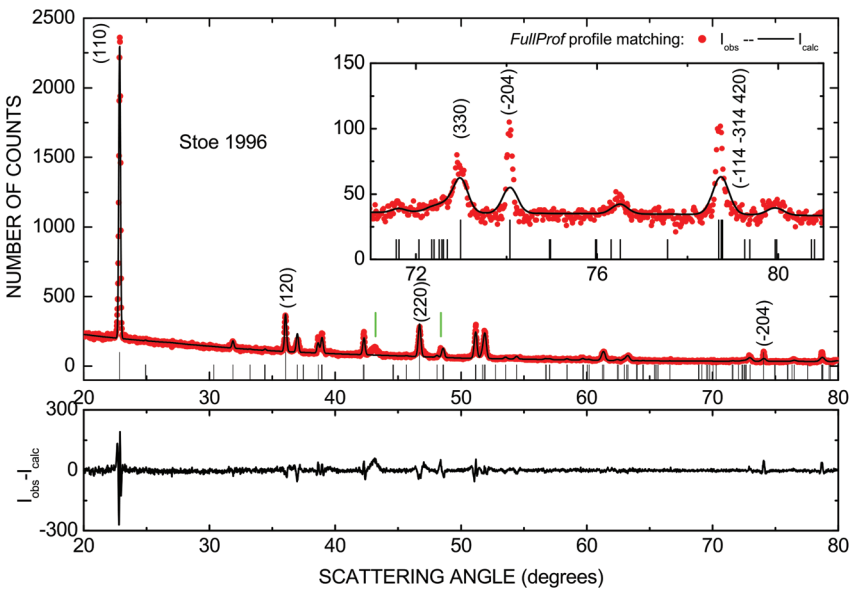

Fig. 1 Powder X-ray diffraction pattern of copper(II) oxalate (sample 1, λ = 1.54056 Å) showing observed (●) and calculated patterns (upper panel, black curves) and the corresponding difference plot (lower panel). Two unidentified impurity reflections at 2θ = 43.2° and 2θ = 48.4° are marked by the green bars above the pattern. The profile-matching mode (Le Bail) was applied to the sample peaks in the program FullProf[15] and the resulting unit cell parameters in the space group $P12_1/n1$ are a = 5.9576(3), b = 5.6091(3), c = 5.1138(2) Å, β = 115.330(4)°. The ticks below the diffraction pattern mark the possible Bragg angle positions for the space group $P12_1/n1$. The profile parameters used for the curves I_{calc} are described in section 4.2 and listed in Table 3.

With limited success, attempts were made to improve the crystallite size by hydrothermal treatment of the product (sample 1). When heated hydrothermally in water at 175 °C for 24 hours, the result was copper(II) oxalate with a slightly increased crystallite size. After 120 hours at 175 °C the result was copper(II) oxalate with a trace of Cu_2O. When heating the product at 200 °C for 144 hours a redox process converted the sample to Cu_2O, CO and CO_2. A special batch to be used for the neutron diffraction measurements was made using D_2O as the solvent (sample 2). A small portion from this batch was used for the X-ray *in situ* measurements (section 3.3) and recently, a synchrotron X-ray diffraction pattern was also recorded for sample 2.

A third sample of copper(II) oxalate (sample 3) was obtained from the Chemistry Department, Oslo University, Norway and used to obtain the first synchrotron X-ray diffraction pattern. No details about the sample preparation are available, but the diffraction pattern is consistent with those obtained for samples 1 and 2.

3. Experimental details, results and analysis of the diffraction data

3.1. Powder synchrotron X-ray diffraction data

Fig. 2 shows the synchrotron X-ray powder pattern for sample 3. It was recorded at ambient temperature at the Swiss Norwegian beam line at ESRF using a wavelength λ = 1.0981 Å and a 2θ range from 15.00° to 63.00° in steps of 0.01°. The sample was contained in a 0.5 mm diameter glass capillary. This pattern was indexed using the program DICVOL04[14] with peak positions and intensities determined using the program FullProf.[15] The suggested solutions are listed in Table 1 together with the original Schmittler cell.[9] The reliability value M_{20} calculated by DICVOL04 serves as a guide to select the best cell. However, this criterion is not enough because the size of the unit cell must be large enough to allocate space for an integer number of formula units of copper(II) oxalate. Using a density of ~3.29 g cm^{-3}, the Schmittler cell and the solution with the highest value of M_{20} (1) in Table 1 allocate space for only one CuC_2O_4 formula unit. Hence, only the space group symmetry of $P1$ can describe a structure of one formula unit of CuC_2O_4 in the cell of solution 1 with all atoms in general positions. The solution 1 was found when including only the 24 strongest reflections in the DICVOL04 calculation. Including one further very weak reflection at $\sin\theta/\lambda \sim 0.297$ Å^{-1} resulted in the solutions 2 to 5. The DICVOL04 calculations for cell 5 used in the structure calculations index the 24 reflections with $l = 2n$ and the very weak reflection as −1 0 3 corresponding to $l = 2n + 1$. Although solution 5 has a relatively low value of M_{20} , it has the best Le Bail profile match (see section 4.1 for further details). The EXAFS study[12] suggests a $Cu(C_2O_4)Cu$ unit with a Cu–Cu distance of 5.14 Å. The solutions 4 and 5 in Table 1 match this distance and can indeed allocate two $Cu(C_2O_4)Cu$-units along or parallel to the ***c***-axis. Furthermore, they are comparable to the proposed cell for CuC_2O_4 [11] and the crystal structure of β-ZnC_2O_4.[11] The ionic radii for Cu^{2+} (0.73 Å) and Zn^{2+} (0.74) suggest that the two oxalates could have comparable unit cell volumes.

Recently a synchrotron X-ray powder diffraction pattern of sample 2 (Fig. 3) was recorded at ambient temperature at the Swiss Norwegian beam line (SNBL) at ESRF using a wavelength

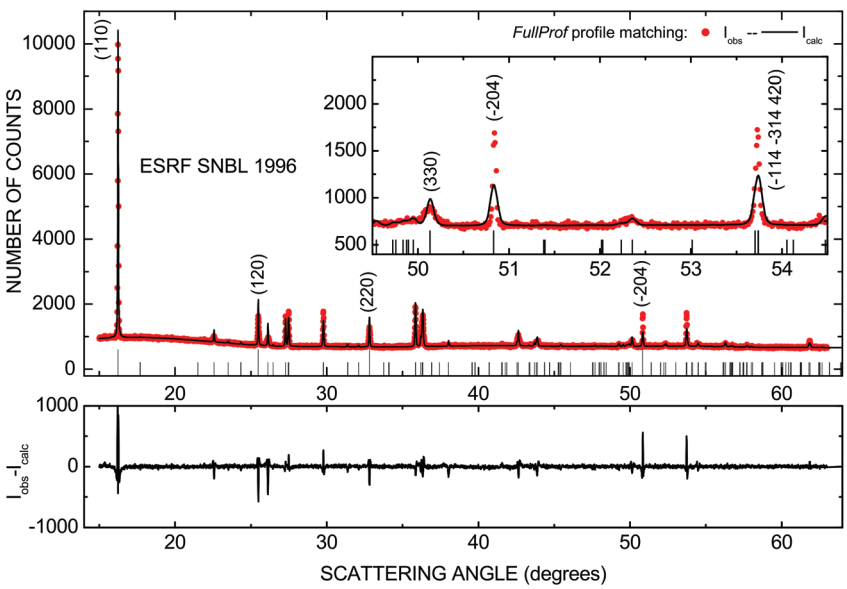

Fig. 2 Powder synchrotron X-ray diffraction pattern of copper(II) oxalate (sample 3, λ = 1.0981 Å) showing observed (●) and calculated patterns (upper panels, black curves) and the corresponding difference plot (lower panel). The profile-matching mode (Le Bail) was applied to the sample peaks in the program FullProf. The unit cell parameters in the space group $P12_1/n1$ are found to be a = 5.9598(1), b = 5.6089(1), c = 5.1138(1) Å, β = 115.320(1)°. The ticks below the diffraction pattern mark the possible Bragg angle positions for the space group $P12_1/n1$. The profile parameters used for the curves I_{calc} are discussed in section 4.2 and listed in Table 3.

Table 1 Unit cell parameters of copper(II) oxalate (sample 3) determined by the indexing program DICVOL04[14] and the powder synchrotron X-ray pattern. The Schmittler cell[9] is listed for comparison. Z is the number of formula units allocated within the cell and M_{20} a figure of merit given by DICVOL04. Although cell 5 has a relatively low value of M_{20}, this cell is used for the final structure refinement because it has the best Le Bail profile match (see sections 3.1 and 4.1)

a (Å)	b (Å)	c (Å)	β°	Volume (Å^3)	Z	M_{20}	Cell/ref.
2.540	5.420	5.550	90°	76.4	1		Ref. 9[a]
5.618(1)	5.384(1)	2.558(1)	90°	77.4	1	47.0	1[b]
5.618(1)	5.384(1)	5.1158(6)	90°	154.7	2	22.9	2
5.609(2)	5.109(2)	5.372(3)	90.16(3)°	153.9	2	12.2	3
6.172(1)	5.384 (1)	5.117(1)	114.44(2)°	154.8	2	28.9	4
5.960(1)	5.618(1)	5.116(1)	115.37(2)°	154.8	2	23.2	5

[a] The suggested space groups for the cell in ref. 9 were *Pmnn* and *P2nn*. The suggested space group for the cell in ref. 4 was *Pnnm*. [b] The cell solution 1 has the space group *Pnnm*.

λ = 0.50483(1) Å and a 2θ range from 3.000° to 50.455° in steps of 0.005°. The sample was contained in a spinning 1.0 mm diameter glass capillary. The wavelength was determined from a Si-0913 powder diffraction pattern (a_{Si} = 5.431021 Å) recorded at SNBL prior to the data collection. The parameters used to model the peak profiles of the three X-ray diffraction patterns are discussed further in section 4.2 and the appendix.

3.2. Powder neutron diffraction data

The neutron powder diffraction pattern of sample 2 is shown in Fig. 4. It was recorded at 5 K using the diffractometer D2B at ILL at a wavelength λ = 1.5949(1) Å and a 2θ range from 9.065 to 157.415° in steps of 0.050°. The sample was contained in a 16 mm diameter vanadium can. The wavelength was determined from the Si-0296 powder diffraction pattern (a_{Si} = 5.431021 Å) recorded at ILL in 1996 prior to the data collection. The parameters used to model the peak profiles of the neutron diffraction pattern are also discussed further in section 4.2 and the appendix.

3.3. *In situ* X-ray diffraction investigation and thermal decomposition

Time-resolved *in situ* synchrotron X-ray diffraction data were collected on the beam line X7B of the National Synchrotron Light Source (NSLS) using a MAR345 area detector. A portion of sample 2 placed in a 0.7 mm diameter quartz glass capillary was heated in a hot air stream by ramping the temperature from 25 °C to 475 °C at a heating rate of 3.17 °C min^{-1}. The X-ray wavelength was λ = 0.9219 Å refined from a powder pattern of LaB_6 (a = 4.1570 Å). The capillary was oscillated 10° to randomise the orientations of the powder grains. The diffraction data frames from the MAR345 area detector were converted to powder patterns (Fig. 5) with the software FIT2D,[16] giving a 2θ range from 0 to 48°.

With a heating rate of 3.17 °C min^{-1} the sequence of 58 (out of 70) powder patterns in Fig. 5 corresponds to 6.5 °C per pattern. The patterns from 1 to 30 show the Bragg reflections of copper(II) oxalate with positions and intensities in agreement with the JCPDS card no. 21-297 for Moolooite. Between the patterns 30 and 31, a structural phase transition is

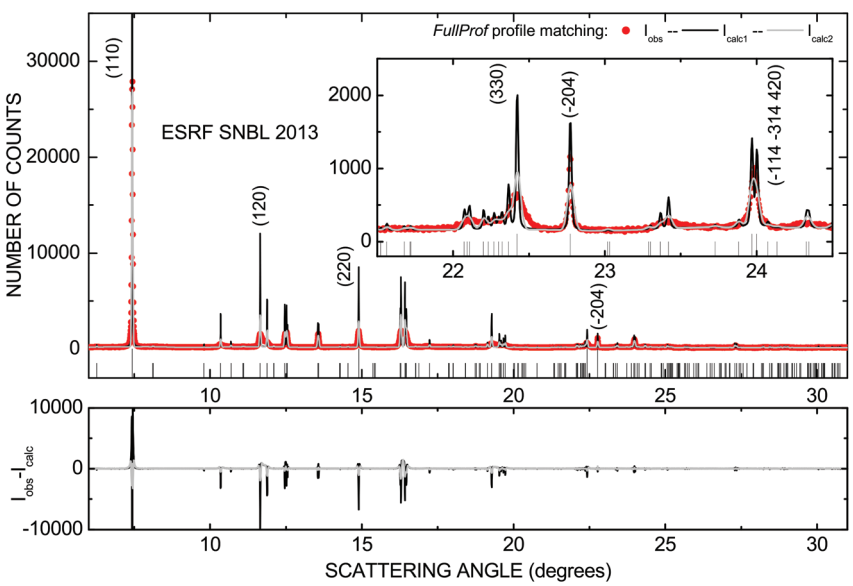

Fig. 3 Powder synchrotron X-ray diffraction pattern of copper(II) oxalate (sample 2, λ = 0.50483(1) Å) showing the observed (●) and calculated patterns (upper panels, black and grey curves) and the corresponding difference plots (lower panel). The profile-matching mode (Le Bail) was applied in the program FullProf and the unit cell parameters in the space group $P12_1/n1$ are found to be a = 5.98713(8), b = 5.59923(7), c = 5.11449(5) Å, β = 115.101(1)°, space group $P12_1/n1$. The profile parameters used for the curves I_{calc1} and I_{calc2} are described in section 4.2 and listed in Table 3. As found for the X-ray diffraction patterns (Fig. 1 and 2) this diffraction pattern shows several high angle narrow peaks. As illustrated in the upper panels these peaks are not satisfactorily modelled by the profile parameters. The ticks below the diffraction pattern mark the possible Bragg angle positions for the space group $P12_1/n1$.

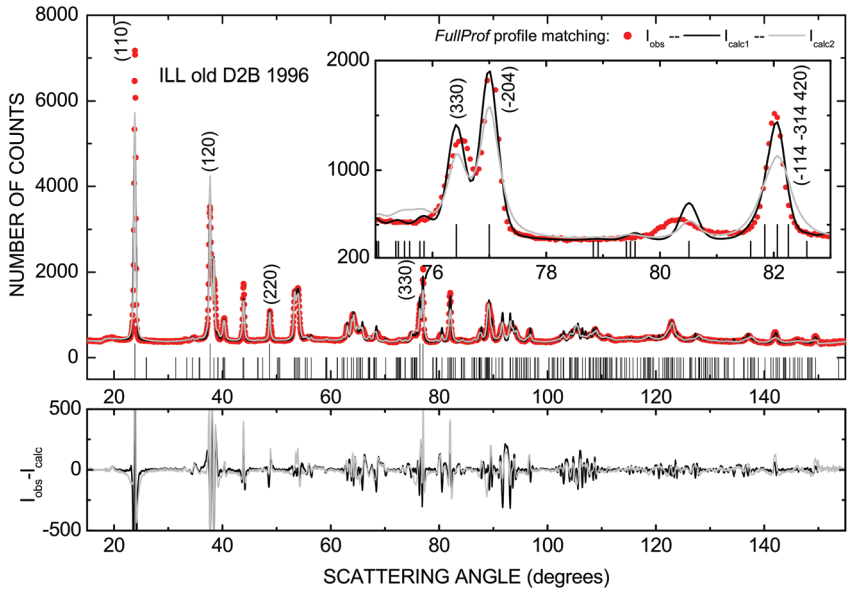

Fig. 4 Powder neutron diffraction pattern of copper(II) oxalate (sample 2, λ = 1.5949(1) Å) showing the observed (●) and calculated patterns (upper panels, black and grey curves) and the corresponding difference plots (lower panel). The profile-matching mode (Le Bail) was applied in the program FullProf and the unit cell parameters in the space group $P12_1/n1$ are found to be a = 5.9569(2), b = 5.5528(1), c = 5.1247(1) Å, β = 115.177(2)°. The profile parameters used for the curves I_{calc1} and I_{calc2} are described in section 4.2 and listed in Table 3. As found for the X-ray diffraction patterns (Fig. 1–3), the neutron diffraction pattern shows several high angle narrow peaks that are not satisfactorily modelled by the profile parameters. The ticks below the diffraction pattern mark the possible Bragg angle positions for the space group $P12_1/n1$.

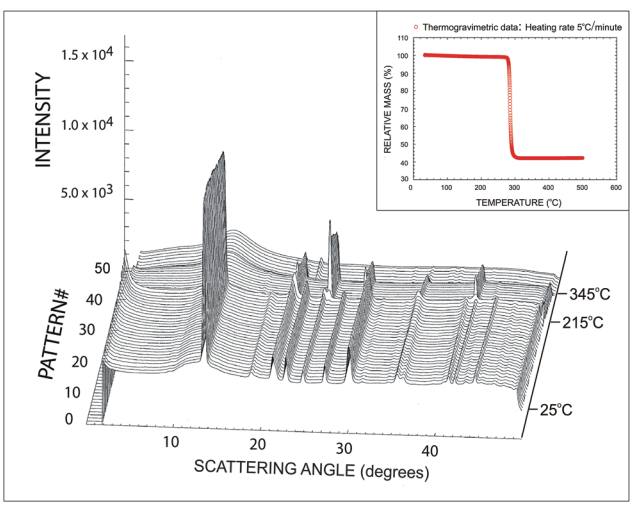

Fig. 5 Sequence of powder patterns (λ = 0.9219 Å) of copper(II) oxalate (sample #2) converting to patterns of Cu_2O at 215 °C and to patterns of CuO at 345 °C. No significant change in the backgrounds of the patterns are observed at the temperatures up to the first phase transition. This indicates that the water previously reported for synthetic copper(II) oxalate[5,6] is not present in the samples investigated in this work. The inset in the upper right hand corner shows the results of a thermogravimetric analysis (sample 2) made in an inert atmosphere at temperatures up to 500 °C using a NETZCH STA 449C instrument. The data show only one phase transition at 280 °C representing the release of C and O with a mass reduction to 42.2%. The calculated reduction for formation of Cu from CuC_2O_4 is 41.9%. Thus there is no indication that the sample contains water. The formation of Cu is in agreement with previous investigations.[6–8]

observed at ~215 °C. This new phase persists in the patterns up to 49 and can be indexed as Cu_2O. Hence, the positions and intensities of the patterns are in excellent agreement with the JCPDS card no. 34-1354 for Cu_2O. The phase transition is driven by a redox process where Cu(II) is reduced to Cu(I), and the oxalate ion is oxidized to carbon dioxide. A third phase transition is observed in pattern 50 at ~345 °C where Cu_2O is oxidized to CuO in a narrow temperature range. The peak positions and intensities of this phase in the patterns are in excellent agreement with the JCPDS card 45-937 for CuO.

The above results are in contrast to the reported differential thermal analysis (DTA) and thermogravimetric analysis (TG) measurements,[17] where the data were interpreted as reduction of $CuC_2O_4{\cdot}0.5H_2O$ to Cu metal and Cu_2O somewhere between 185 and 300 °C , which was followed by oxidation so that Cu_2O and CuO were present in the temperature range 300 °C to 345 °C, and finally only CuO was present at temperatures above 345 °C.[17] The formation of metallic Cu in the first reaction is rather speculative. The most likely redox process after the water molecules have escaped is:

$$2CuC_2O_4 \rightarrow Cu_2O + CO + 3CO_2$$

and the oxidation process:

$$Cu_2O + 1/2O_2 \rightarrow 2CuO$$

The present kinetic study of the thermal decomposition of copper(II) oxalate did not reveal evidence for the formation of a copper(I) oxalate as an intermediate compound in the decomposition.[8] This would have been most unlikely,

considering the well-known reducing potential of the oxalate ion. In aqueous media it is also well known that Cu(II) is reduced to Cu(I). An example is the red Cu_2O obtained in Fehling's test for sugar molecules. The present investigation definitely shows that Cu_2O is present in the solid-state reaction as a pure phase in the temperature range 215 °C to 345 °C when heated in air. In contrast we find from the thermogravimetric measurements performed in argon with a heating rate of 5 °C min^{-1}. that sample 2 contains no crystal water and reduces to pure Cu in a narrow temperature range around 295 °C (see insert in Fig. 5).

3.4. Measurements of magnetic susceptibility

Early magnetic studies of copper(II) oxalate revealed a weak magnetic response.[18–20] The magnetic susceptibility in the temperature range 100 to 350 K showed a broad maximum at 260 K that was suggested to result from linear chains of interacting antiferromagnetically coupled Cu(II)-dimers. Similar quasi-one-dimensional spin chain structures have been observed in $Na_3Cu_2S_bO_6$,[21–23] Cu_5SbO_6,[24] $LiCuSbO_4$ [25] and in $CuCl_2$.[26] In contrast to $CuCl_2$ which orders antiferromagnetically with T_N = 23.9 K the other systems including CuC_2O_4 do not show signs of magnetic ordering.

In the present work, the magnetic susceptibility of copper(II) oxalate (sample 2) was measured by vibrating sample magnetometry (VSM) in the temperature range 2 to 300 K and a magnetic field of 0.537 T (5.37 kG) using a cryogenic free measurement system (CFMS) from CRYGENIC Ltd. The set point of the applied field was chosen to be well within the linear response to the field and the actual value of the field determined by a Hall probe. The susceptibility in units of μ_B/T per Cu atom is shown by the open circles in Fig. 6. It has a broad maximum around 260 K as previously reported and a Curie tail at low temperatures without any indication of a magnetic order. The data have been analysed using a combination of the following three terms:

a Curie–Weiss term $\chi_{CW} = A/(T + \theta_{CW})$,

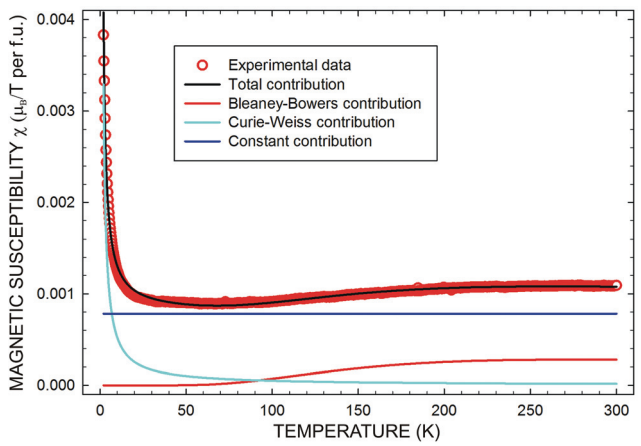

Fig. 6 Magnetic susceptibility of copper(II) oxalate (sample 2) measured in a magnetic field of 0.537 T (5.37 kG). The three terms used to analyse the susceptibility are discussed in detail in section 3.4.

a constant paramagnetic contribution $\chi_{constant} = C$ and

a Bleaney–Bowers expression $\chi_{BB} = D/(k_BT(3 + \exp(\Delta/T))$, where θ_{CW} is the Curie–Weiss temperature and the Bleaney–Bowers expression represents the broad features of the susceptibility at higher temperatures, resulting from antiferromagnetically coupled Cu^{2+}–Cu^{2+} spin-1/2 dimers with a singlet–triplet splitting of Δ. Although the Bleaney–Bowers expression represents the susceptibility of isolated Cu-dimers, it may, to a good approximation, simulate the magnetic susceptibility of magnetic linear chain structures with an energy gap and weak dispersion in the excitation spectrum as exemplified in ref. 21.

In the absence of a microscopic model for the magnetic interactions, we therefore use this expression to fit the data. The result of the combined fit to $\chi = \chi_{CW} + \chi_{constant} + \chi_{BB}$ is shown as the black curve in Fig. 6. The Curie–Weiss contribution is the cyan curve, the constant contribution is the blue line and the Bleaney–Bowers contribution is the thin red curve. The Curie–Weiss temperature is $\theta_{CW} = -0.48(2)$ K indicating that the low temperature Curie tail represents essentially free spins. From analyses of the Curie–Weiss constant A we find that the relative concentration of free copper spins is only 0.66% and may result partly from uncompensated spins at the surface of the nano-sized crystallites. Analyses of the Bleaney–Bowers contribution give an energy gap of Δ = 442(3) K and a relative concentration of Cu^{2+} spins in dimers equal to 20.3(2)%. Thus a significant part of the spins is not accounted for by the Curie–Weiss and Bleaney–Bowers contributions. This is consistent with the fact that the constant susceptibility $\chi_{constant}$ = $2.171(5) \times 10^{-6}\mu_B/T$ per Cu atom is quite large. It remains a challenge to explore the origin of this large constant paramagnetic susceptibility and its relation to the apparently large concentration of Cu-spins not accounted for. However, it is confirmed that the magnetic susceptibility measurements do not show any sign of magnetic order down to 2 K.

4. Crystal structure analysis of synchrotron X-ray and neutron diffraction data

4.1. Space group selection by Le Bail profile-matching

The profile Le Bail matching mode of the program FullProf[15] was applied to the powder diffraction synchrotron X-ray pattern (Fig. 2 sample 3) in order to distinguish between the DICVOL04 unit cell solutions 4 and 5 of Table 1 with reliability factors M_{20} = 28.9 and 23.2, respectively. When using the space group $P2_1/c$ (#14) in the $P12_1/n1$ setting, the solution 4 gave the reliability value R_{Bragg} = 5.66, χ^2 = 2.49 and unit cell parameters a = 6.172(1), b = 5.384(1), c = 5.117(1) Å, β = 114.49(2)° . Similarly, the solution 5 gave the reliability value R_{Bragg} = 5.24, χ^2 = 2.14 and unit cell parameters a = 5.960(1), b = 5.618(1), c = 5.116(1) Å, β = 115.37(2)°. Of these two monoclinic solutions cell 5 has the highest reliability value for the Le Bail FullProf profile-matching calculation. More importantly, the solution index observed a group of reflections as $0k0$ with $k = 2n$ which

is not the case for the Le Bail FullProf profile-matching when using cell 4. This fact supports the use of the space group 14 in the $P12_1/n1$ setting, which is consistent with the β-ZnC_2O_4 crystal structure.[11] Therefore, the DICVOL04 cell 5 is used in the further crystal structure analysis reported below.

4.2. Instrumental resolution and profile parameters for the X-ray and neutron pattern

The peak positions by FullProf are well matched both for cells 4 and 5, but close inspection of Fig. 2 reveals that the profile matching of the CuC_2O_4 Bragg peaks is rather poor. Some of the reflections are broad and some are narrow as seen in the inset of the upper panel. As examples, the reflections (−2 0 4) and the group of three overlapping peaks (−1 1 4), (−3 1 4) and (4 2 0) are very sharp, with almost the same widths as the low angle and strongest (1 1 0) reflection in the pattern while the (3 3 0) peak close to (−2 0 4) is quite broad. The group of peaks observed in the region between the narrow (1 2 0) and (2 2 0) reflections also show irregular variation of peak widths. A similar behaviour is observed in the insets of Fig. 1, 3 and 4. Instrument calibration resolution parameters are unavailable for the X-ray patterns in Fig. 1 and 2. Therefore, the best available profile parameters for structure refinements are those deduced from FullProf matching of the pseudo Voigt Bragg peaks from the sample (Npr = 7) listed in italics in Table 3 in the appendix. Generally, these parameters match the profiles of the narrow peaks rather poorly and hence do not describe the instrumental resolution. Despite *R*-factors of the order of 70 in attempts to refine a model crystal structure using these profile parameters (see section 4.4), the refinements allow a clear distinction between solutions 4 and 5 (Table 1).

The recent synchrotron X-ray powder diffraction pattern of sample 2 (Fig. 3) was recorded at the same time as the Si-0913 pattern in order to get sample independent profile parameters determined from the Si-pattern using FullProf[15] in the profile-matching mode. The refinement of the Si-0913 pattern was done in a three stage process using the pseudo-Voigt line shape (Npr = 7) where *U*, *V* and *W* were first refined with $X = Y = 0$ followed by refinement with fixed *U*, *V* and *W* and variable *X* and *Y* parameters. Finally, the five pseudo-Voigt line shape parameters were all refined to give the best possible modelling of the Si pattern for all observed peaks with $d > 0.64$ Å. The resulting profile parameters for the refined Si-0913 diffraction pattern are given in normal characters in Table 3. Fig. 12a of the appendix displays the corresponding diffraction pattern.

The result of the profile matching of the synchrotron X-ray data for the CuC_2O_4 sample 2 using the profile parameters derived from the Si pattern is shown as I_{calc1} (black curves) in Fig. 3, which reproduces the observed I_{obs} pattern reasonably well. The profile parameters fit the narrow (−2 0 4) and the group of (−1 1 4), (−3 1 4) and (4 2 0) peaks well but this is not the case for several other peaks. In particular, the area of the observed (1 1 0) peak corresponds roughly to the calculated peak area, but the ratio between the calculated and observed peak heights is ∼2 ,with the ratio between the observed and calculated widths being ∼1/2. An attempt to estimate profile parameters from the sample peaks is shown as I_{calc2} (grey curves) and listed as "a clever guess" with numbers in italics in the fourth column of Table 3.

The first attempts to match the Bragg peak profiles of the neutron pattern resulted in pseudo Voigt (Npr = 7) profile parameters close to the parameters used in the structure analysis of $[Bi_6O_4(OH)_4]_{0.54(1)}[Bi_6O_5(OH)_3]_{0.46(1)}(NO_3)_{5.54(1)}$,[27] where the neutron diffraction pattern was also recorded using D2B. Therefore, it seemed justifiable to use the profile parameters from ref. 27 as sample independent profile parameters in the present study. However, as found for the X-ray data, the profiles with an unsystematic combination of broad and narrow peaks could not be matched satisfactorily. Instead, sample independent profile parameters determined from the Si-0296 pattern could be used. The resulting instrument parameters and the refined Si diffraction pattern are given in Table 1 and Fig. 12b in the appendix. The result of the profile matching of the neutron diffraction data for the CuC_2O_4 sample 2 using the profile parameters derived from the Si pattern is shown as I_{calc1} (black curves) in Fig. 4. The parameters fit the narrow (1 2 0), (2 2 0), (−2 0 4) and the overlapping (−1 1 4), (−3 1 4), (4 2 0) peaks well, and in contrast to the corresponding X-ray data for sample 2 the observed (1 1 0) peak is also reasonably well reproduced. A calculated pattern using an estimate of the profile parameters from the sample peaks is shown as I_{calc2} (grey curves in Fig. 4) and listed as "ref. 27 with *Y*" with numbers in italics in the fifth column of Table 3.

From the above it is obvious that none of the sets of profile parameters matches the observed Bragg peaks satisfactorily. However, it is also obvious that the three samples have consistent X-ray patterns and that the mixture of broad and narrow Bragg peaks is quite similar for the two types of radiation. The possible common source of the observed variation of line widths may be disordered stacking faults and/or microstructural size and/or strain effects in the samples, and this has to be considered in the final crystal structure analysis (section 4.4) where the sample independent profile parameters from the X-ray (Si-0913) and neutron (Si-0296) Si diffraction patterns are used.

4.3. Search for structure solution and D_2O molecule by *ab initio* calculations and refinements

An *ab initio* structure solution using the program FOX[28] followed by structure refinements using FullProf[15] gave a solution with $R_{Bragg} = 17.93$, $R_F = 11.57$, $\chi^2 = 72.5$ for the neutron diffraction pattern of sample 2. The model suggested by FOX is a model where Cu atoms are placed in (2a) sites and the oxalate ions are placed with their symmetry centres at (2b) sites of $P12_1/n1$. However, the calculated pattern for this model has a number of unobserved additional minor reflections and does not account for a large fraction of the intensity in some of the stronger reflections.

It has been reported that Moolooite as well as synthetic copper(II) oxalate contain water.[3,4,9,10] Using FOX,[28] attempts were therefore made to locate a possible water (D_2O) molecule

and an additional scattering contribution was indeed observed close to the Cu-atom position. This eliminated some of the minor reflections in the calculated pattern, and the resulting reliability values were R_{Bragg} = 17.48, R_F = 11.28, χ^2 = 63.7, but, the D_2O molecule predicted by Fox was found too close to the Cu atom site to be plausible. However, the neutron scattering lengths and the atom distances in a D_2O molecule and in a half $C_2O_4^{2-}$ ion are comparable.[29] Therefore, it seemed just as plausible to assume that the additional scattering at the Cu-atom site position originated from random stacking faults of an oxalate ion placed close to the Cu-atom positions.

4.4. Final structural model including stacking faults and microstructural size and strain effects

The combined *ab initio* FOX calculation and FullProf refinement mentioned above strongly suggested that the compound contained no water, but rather two randomly occupied Cu and oxalate sites. In order to test this hypothesis, stacking faults were introduced in a $P12_1/n1$ setting with half the Cu atoms at (2a) and the other at (2b). Half the oxalate ions could then have coordinates x, y, z (4e), and the other half could have coordinates x', y', $z' = x$, y, $z + 1/2$ (4e). In such a refinement, the oxalate ions have their centres of symmetry at the sites (2b) and (2a), respectively, and the oxalate coordinates x', y', z' are restrained to have the values x, y, $z + 1/2$. However, if the occupancies of the oxalate-ions are allowed to vary, the latter need not be the case. Refinement by FullProf resulted in a solution with reliability values R_{Bragg} = 56.1, R_F = 29.8, χ^2 = 36.4 shown as the grey curve at $I_{calc,2cryst,\ nosize\ or\ strain}$ in the upper panels of Fig. 7. The resulting atomic coordinates, isotropic temperature factors, occupancies and inter atomic distances are listed in Table 2.

The relatively high value of χ^2 is mainly due to a misfit of the narrow reflections discussed in section 4.2. Therefore, the microstructural parameters for size and strain were included and refined in two steps. The first step was refinement to convergence of nine size parameters with fixed structural parameters (R_{Bragg} = 10.9, R_F = 9.3, χ^2 = 6.3) and the second refinement to convergence of nine strain parameters with fixed structural and size parameters (R_{Bragg} = 8.8, R_F = 8.0, χ^2 = 5.2). Repeated refinements did not improve the overall agreement. In these refinements the microstructural parameters were included in the form of spherical harmonic parameters for Laue class 2/*m* (size-model = 15 and strain model = 2). These parameters are also listed in Table 2 and the resulting model diffraction pattern is shown as the black curve marked $I_{calc,2cryst}$ in the upper panels of Fig. 7. Although the corresponding difference pattern ΔI_{2cryst} shown in the lower panel of Fig. 7 is considerably improved compared to $\Delta I_{nosize,nostrain}$ there was no significant change of the dominant structural parameters (atom coordinates, temperature factors and crystallite occupancy) when allowing them to vary. The main effect of including size and strain analysis is a significantly better fit of the line shapes.

As a further support for the stacking fault model structure, Fig. 8 shows a comparison between the neutron diffraction patterns with and without stacking faults including size and strain parameters. In the upper panels, the black curve marked $I_{calc,2cryst}$ refers to the final structural model (also shown in Fig. 7) with two randomly stacked Cu-oxalate

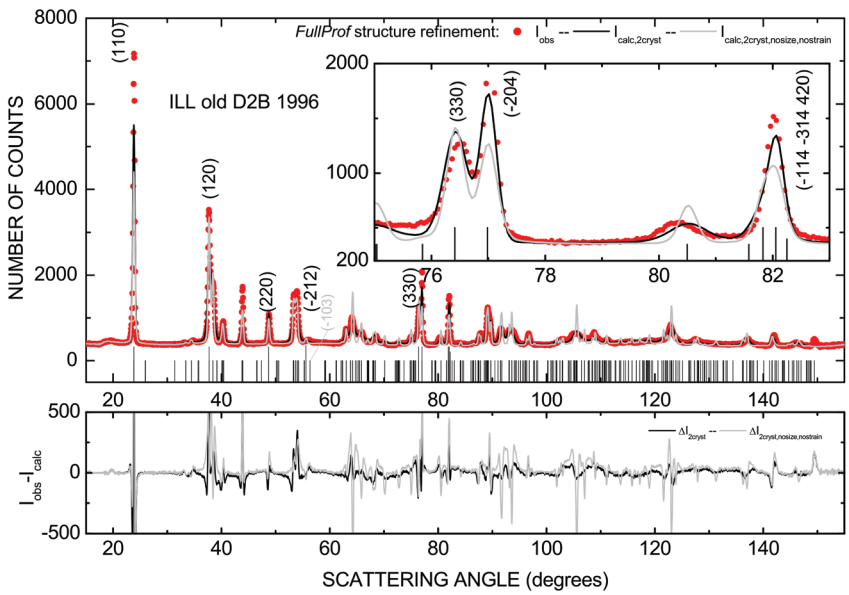

Fig. 7 Powder neutron diffraction pattern of copper(II) oxalate (sample 2, λ = 1.5949(1) Å) showing the observed (●) and the refined patterns. In the upper panels, the black curves marked $I_{calc,2cryst}$ refer to the structural model for CuC_2O_4 with two Cu-oxalate crystallites randomly stacked along the *c*-axis. See section 4.4 and Table 2 for further details. The grey curves marked $I_{calc,2cryst,nosize,nostrain}$ refer to the same structural parameters, but do not include peak broadening caused by size and strain effects. The lower panel shows the corresponding difference patterns ΔI_{2cryst} and $\Delta I_{2cryst,nosize,nostrain}$. The unit cell and profile parameters are listed in Table 3 (column 5, normal characters). The ticks below the diffraction pattern mark positions of the allowed Bragg peaks for the structural model listed in Table 2.

Table 2 Atomic coordinates calculated by FullProf refinement of the neutron diffraction pattern. The unit cell parameters are a = 5.9569(2), b = 5.5528(1), c = 5.1247(1) Å, β = 115.177(2)° space group $P2_1/c$ (#14) in the $P12_1/n1$ setting. The nearest neighbour inter atomic distances and the size and strain parameters for Laue Class 2/m are also listed

Atom	x/a	y/b	z/c	B_{iso}	Occ.
Atom coordinates for the CuC_2O_4 crystallite centre at (2a)					
Cu1	0.000	0.000	0.000	0.8(2)	0.500
O1	0.162(1)	0.165(1)	0.803(2)	0.4(2)	1.000
O2	0.215(1)	0.155(2)	0.396(2)	0.4(2)	1.000
C1	0.109(1)	0.093(1)	0.553(2)	0.8(1)	1.000
Atom coordinates for the CuC_2O_4 crystallite centre at (2b)					
Cu2	0.000	0.000	0.500	0.8(2)	0.500
O3	0.162(1)	0.165(1)	1.303(2)	0.4(2)	1.000
O4	0.215(1)	0.155(2)	0.896(2)	0.4(2)	1.000
C2	0.109(1)	0.093(1)	1.053(2)	0.8(1)	1.000
Nearest neighbour inter atomic distances in Å					
Cu1–O1	1.918(8)	C1–O1	1.26(1)	C1–C1′	1.576(6)
Cu1–O2	2.081(7)	C1–O2	1.27(1)		
Anisotropic size parameters for Laue class 2/m (size-model = 15)					
Y00	4.50	Y20	1.39	Y22+	−2.19
Y22−	1.76	Y40	5.32	Y42+	2.93
Y42−	−3.63	Y44+	1.33	Y44−	0.15
Anisotropic strain parameters for Laue class 2/m (strain-model = 2)					
S_400	11.46	S_040	5.45	S_004	1.94
S_220	−13.14	S_202	24.13	S_022	−5.47
S_121	−16.98	S_301	26.42	S_103	10.57

molecules along the ***c***-axis while the grey curve marked $I_{calc,1\text{-}cryst}$ refers to the original structural model[11] with just one ordered Cu-oxalate crystallite scaled to match the calculated intensity in the first Bragg peak (1 1 0) at $\sin\theta/\lambda \sim 0.129$ Å^{-1}. The lower panel shows the corresponding difference patterns ΔI_{2cryst} and ΔI_{1cryst}. The effect of introducing the stacking faults is obvious because a number of weak $l = 2n + 1$ peaks in $I_{calc,1cryst}$ for the crystallite with Cu at 2a can be wiped out by destructive interference with the corresponding contributions from the 180° out-of-phase crystallite with Cu at 2b. It should be noted that complete cancellation of the $l = 2n + 1$ reflections occurs only if the oxalate ions have identical occupancies and identical x and y site coordinates for the O and C atoms. The present data can indeed be refined when including varying occupancies and different x and y site coordinates for the O and C atoms. However, within reasonable limits the site positions and the R-factors are only marginally changed, and once the size and strain effects are included the intensity of the broadened −1 0 3 reflection is barely visible in the calculated pattern (Fig. 7 and 9).

As a supplement to the neutron diffraction patterns in Fig. 7 and 8, Fig. 9 shows the calculated X-ray diffraction pattern using the same structural parameters as used for the neutron pattern (Table 2). The values for the size and strain parameters are listed in Table 4. They are rather different from those found in the neutron case as discussed further in section 4.5. The reliability factors for the modelling of the synchrotron X-ray data have higher values than found for the neutron data, but follow the same sequence (R_{Bragg} = 67.9,

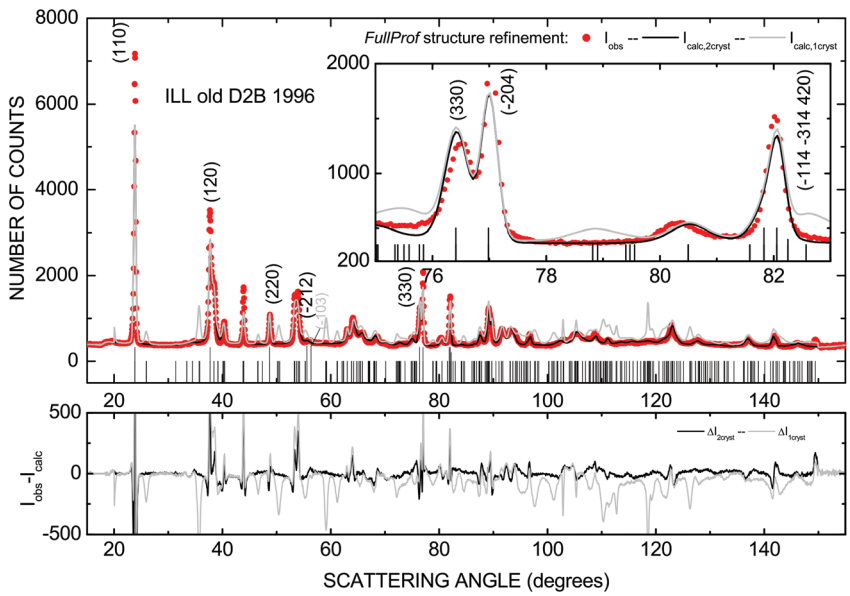

Fig. 8 Comparison of the powder neutron diffraction pattern of copper(II) oxalate (sample #2, λ = 1.5949(1) Å) showing observed (●) and refined patterns of structural models. In the upper panels, the black curves marked $I_{calc,2cryst}$ refer to the structural model with two Cu-oxalate crystallites randomly stacked along the c-axis and shown in Fig. 7. The grey curves marked $I_{calc,1cryst}$ refer to a structure similar to the one proposed for β-ZnC_2O_4 [11] with just one ordered Cu-oxalate crystallite (see section 4.4 for further details). The lower panel shows the corresponding difference patterns ΔI_{2cryst} and ΔI_{1cryst}. The unit cell, profile parameters and the parameters for anisotropic peak broadening due to size and strain are the same as those used in Fig. 7. The ticks below the diffraction pattern mark the positions of the allowed Bragg peaks for a structural model with only one of the crystallites listed in Table 2.

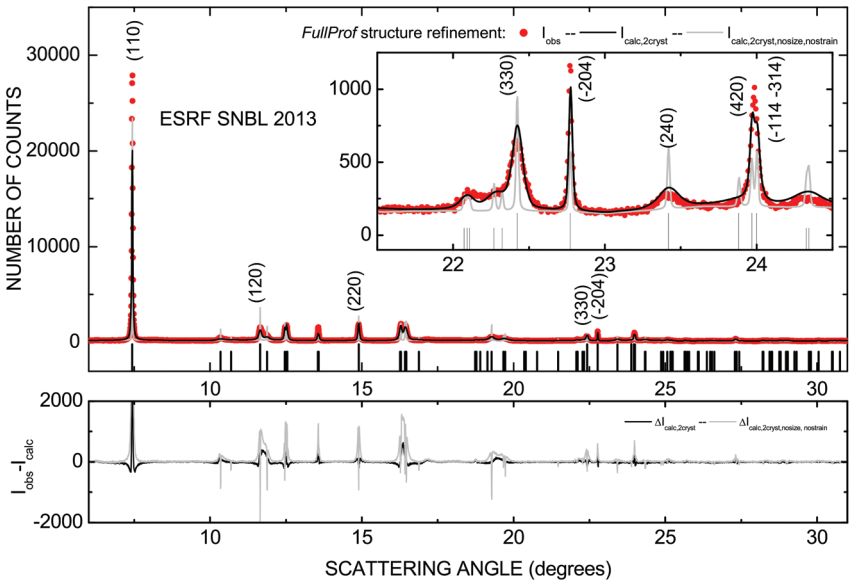

Fig. 9 Powder synchrotron X-ray diffraction pattern of copper(II) oxalate (sample #2, λ = 0.50483(1) Å) showing observed (●) and calculated patterns using the structural parameters found by refining the neutron data as described in detail in section 4.4 (Fig. 7, Table 2). In the upper panels, the black curves marked $I_{calc,2cryst}$ refer to the calculated pattern including the anisotropic peak broadening caused by size and strain which is somewhat different from that found for the neutron data (see section 4.5). The grey curves marked $I_{calc,2cryst,nosize,nostrain}$ refer to the calculated pattern without size and strain peak broadening. The lower panel shows the corresponding difference patterns $\Delta I_{calc,2cryst}$ and $\Delta I_{calc,2cryst,nosize,nostrain}$. The unit cell and profile parameters are listed in Table 3 (column 4, normal characters). The ticks below the diffraction pattern mark positions of the allowed Bragg peaks for the structural model listed in Table 2.

R_F = 43.2, χ^2 = 38.6; R_{Bragg} = 15.7, R_F = 18.4, χ^2 = 6.7; R_{Bragg} = 14.5, R_F = 18.1, χ^2 = 5.7).

4.5. Comments on the microstructure size and strain analysis by FullProf

Obviously, Fig. 7–9 and the agreement factors listed in section 4.4 indicate that the overall agreements between the observed and calculated diffraction patterns are significantly improved by including the micro size and strain analysis. However, there are large correlations between the nine parameters for size and the nine parameters for strain and their actual values are extremely dependent on even minor changes in the profile parameters. Therefore, it is difficult to judge how meaningful these parameters are, but as mentioned in section 4.4 they have no significant influence on the atom coordinates, temperature factors and crystallite occupancy.

As examples, Fig. 10 shows a summary of the resulting microstructural analysis for one of the first attempts to include these additional parameters in the refinement of the ILL neutron data (Fig. 7) and the corresponding data for the final microstructural analysis for the ESRF synchrotron X-ray data (Fig. 9). The corresponding microstructure parameters are in Table 4. The profile parameters used for the microstructural analysis of the synchrotron X-ray data are those listed in normal characters in column 4 of Table 3 and shown as downwards pointing green triangles in Fig. 13 in the appendix, *i.e.* the parameters are the ones determined from the Si-0913 SNBL calibration data for the instrument. The corresponding microstructural analysis is shown as the contours marked by circles in Fig. 10.

A similar approach could not be used for the microstructural analysis of the neutron data. The reason is obvious when comparing the resolution functions determined by profile matching of the Si patterns (supposed to represent the instrumental resolution) and the resolution functions determined by profile matching of the CuC_2O_4 sample patterns determined from the synchrotron X-ray data and the neutron data, respectively. These two data sets are shown as the green triangles (Si data) and the red triangles (CuC_2O_4 data) in Fig. 13. In the X-ray case, the resolution function for the CuC_2O_4 pattern lies well above that of the Si pattern. In the neutron case, there is a crossover of the two curves at $2\theta \sim 70°$, which means that the resolution function for the Si pattern lies above that of the CuC_2O_4 pattern at low angles. In other words, the widths of the intense low angle peaks are not matched by the profile parameters determined for the Si-0296 calibration pattern (listed in normal characters in column 5 of Table 3). This means that most of the reflections were rejected by FullProf as resolution limited in the microstructural analysis when using the supposed instrumental resolution parameters. However, the first microstructural analysis was done using the neutron data, and at the time, the Si-0296 calibration data were not yet available to us, so instead the profile parameters listed in italics in column 5 of Table 3 were used. These profile parameters are close to the values used in ref. 27 and this microstructural analysis by FullProf seemed to give rather meaningful results without resolution limited rejected peaks.

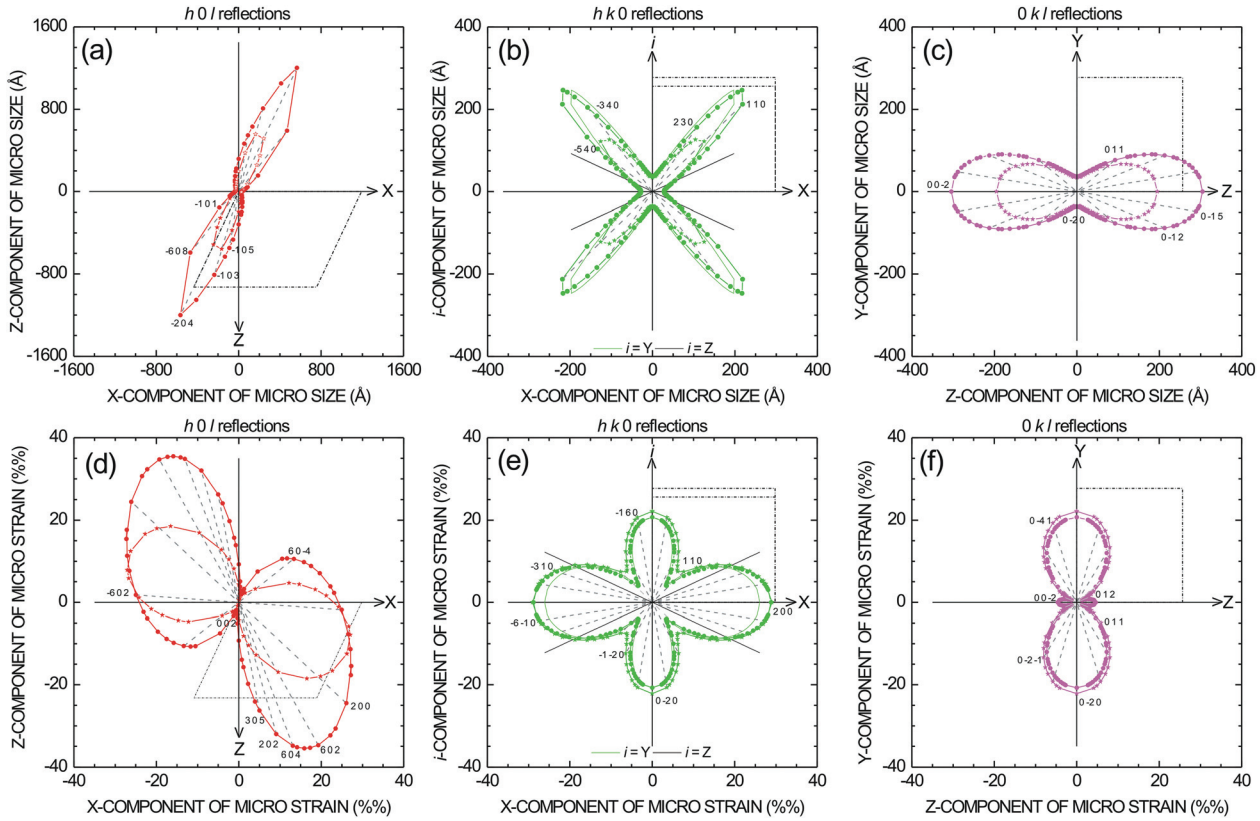

Fig. 10 Summary of the FullProf analyses of micro size (a–c) and strain (d–f) synchrotron and neutron diffraction data. The contours in a, d, c and f show the projections of the micro size and strain on the *ac*- and *bc*-planes (*XZ* or *YZ* orthogonal axes), respectively. The circles represent synchrotron data and the stars, neutron data. The thin line green contours and the black straight lines in (b) and (e) are the micro size and maximum strain projections (X-ray data only) in the *XY*- and *XZ*-planes that combine to the thick green contours with circles in the *a***b*-plane. The dot-dashed parallelepipeds (arbitrary scale) mark the shape of the unit cell in the different projections. Note the factor of four between the scales in (a), (b)., and (c). The numbers at one of the endpoints of the symmetry related grey dashed lines are Miller indices for some of the reflections with observed and calculated X-ray or neutron intensity. See section 4.5 for further details.

Table 3 Summary of profile parameters used. The parameters determined by FullProf profile matching of the CuC_2O_4 diffraction peaks shown Fig. 1 and 2 are listed in italics. For the CuC_2O_4 patterns shown in Fig. 3 and 4, Si calibration diffraction patterns were made at the time of the data collection and the profile parameters are determined from these patterns (Fig. 12(a) and 12(b)) and listed in normal characters. Two additional sets of profile parameters (listed in italics) were determined from profile matching of the CuC_2O_4 peaks. In column 4 they are called "a clever guess" and in column 5 they are determined using the *U*, *V*, *W* from ref. 27 and refinement of *Y*. The CuC_2O_4 profile parameters were determined using the wavelengths listed below

	Sample 1	Sample 3	Sample 2	Sample 2
Radiation	Cu-Kα_1 Aarhus University	Synchrotron X-rays ESRF	Synchrotron X-rays ESRF	Neutrons ILL
Instrument	STOE 1996	SNBL 1996	SNBL 2013	D2B old 1996
Calibration	By sample	By sample	Si-0913 SNBL *a clever guess*	Si-0296 D2B *ref. 27 with Y*
λ (Å)	1.54056	1.0981	0.50483(1)	1.5949(1)
a (Å)	5.9576(3)	5.9598(1)	5.98713(8)	5.9569(2)
b (Å)	5.6091(3)	5.6089(1)	5.59923(7)	5.5528(1)
c (Å)	5.1138(2)	5.1138(1)	5.11449(5)	5.1247(1)
β (°)	115.330(4)	115.320(1)	115.101(1)	115.177(2)
U	*0.222(8)*	*0.0310(1)*	0.0042(9), *0.02*	0.073(13), *0.08*
V	*0.0017(15)*	*−0.0050(2)*	0.00004(1), *0.0013*	−0.24(4), *−0.09*
W	*0.0153(6)*	*0.0011(3)*	0, *0.002*	0.24(3), *0.060*
X	*0*	*0*	0.0036(6), *0*	0.013(45), *0*
Y	*0*	*0.0258(3)*	0.0076(6), *0*	0.072(35), *0.243*
Figure reference	Fig. 1	Fig. 2	Fig. 3	Fig. 4

The corresponding microstructural analysis is shown by the contours marked by stars in Fig. 10.

The results of the microstructure are summarised as contours in three projections for microstructural size (a–c) and strain (d–f). In Fig. 10, the *X*-axis coincides with ***a***, the *Y*-axis with ***b*** and ***b**** and the *Z*-axis with ***c****, where ***a***, ***b*** and ***c*** are the real cell vectors and ***a****, ***b**** and ***c**** are reciprocal cell vectors. In the *XZ*-plane ***c*** and ***a**** are at $\gamma = \beta - 90°$–25.1° to the *Z*- and *X*-axes, respectively. This means that Fig. 10a, c, d and f show the true projections in the *XZ*- and *ZY*-planes, respectively, while the thick green curves in Fig. 10b and e show the projection in a plane tilting the angle γ out of the paper plane around the *X*-axis. There are two sets of contours in each subfigure. The stars are for the neutron data and the circles for the synchrotron X-ray data. The shapes of the contours are almost similar, but the values are different especially those for the micro sizes. The reason for this difference is not clear, but probably related to the uncertainty about the resolution curve used in the analysis of the neutron data.

5. Conclusion

The copper oxalate mineral Mooloolite[3] has been reported to have the composition $CuC_2O_4{\cdot}0.44H_2O$. However, a reported high resolution thermo gravimetric analyses and hot stage Raman spectroscopy have shown that the mineral Mooloolite decomposes at 250 °C, and that no water is released in the mass loss.[30] The decomposition temperature is slightly higher than the 215 °C found in this investigation (see Fig. 5). Nano-sized crystals of copper(II) oxalate obtained in aqueous media by precipitation of Cu(II) solutions with oxalate containing solutions have been reported to have compositions $CuC_2O_4{\cdot}xH_2O$ with x from 0.3 to 1.0.[19] The present investigation including *in situ* synchrotron powder X-ray diffraction thermal decomposition data, thermogravimetric analysis and neutron powder diffraction structure analysis did not support a H_2O/D_2O content in the compound. Copper(II) oxalate is not stable during dry and hydrothermal heat treatments where it converts to Cu_2O. The neutron diffraction data and subsequent magnetic susceptibility measurements on the same sample did not show any magnetic order in the investigated temperature range 2–300 K.

The determined crystal structure is similar to that of β-ZnC_2O_4 [11], although the β-ZnC_2O_4 structure does not include stacking faults. The crystal structure of CuC_2O_4 determined in the present neutron and X-ray diffraction structure analysis has planar CuC_2O_4Cu bands along the ***c***-axis tilted approximately 45° to the ***ac***-plane, and with stacking faults along the ***b***-axis. The Cu–O distances are 1.89(1) Å for O1 and 2.066(8) Å for O2 within the bands, and the Cu–O2 distance is 2.483(9) Å to a copper atom in adjacent bands. The size of the microstructural crystallites is very anisotropic with the corresponding anisotropic strains as shown in Fig. 10.

Fig. 11a displays the projection along the 010-direction of the model structure found in this work for the CuC_2O_4 crystallite with Cu-atoms (Cu1) centred at the (2a) sites in the $P2_1/c$ (14) in the $P12_1/n1$ setting. The grey hatched pentagons indicate the packing of the planar CuC_2O_4 Cu-bands omitting the stacking faults. This model is consistent with the unconfirmed model structure deduced from EXAFS studies.[12,13] In the EXAFS model, a Cu–O distance of 1.98 Å and a Cu–Cu distance of 5.14 Å were suggested, in agreement with the *c*-axis of the unit cell of this work. Further, the Cu–O distances found in the present work are also comparable with the Cu–O distances found in the copper compound $Na_2Cu(C_2O_4)_2{\cdot}2H_2O$. That compound has Cu–O distances of 1.929(1) Å and 1.930(1) Å in the planar complex, and longer Cu–O distances of 2.803(2) Å and 3.576(2) Å.[31] The CuO_6 coordination in the present compound is a deformed octahedron. As examples, Fig. 11b shows one full octahedron and two half octahedra. The bond lengths differ slightly for the two octahedra shown, and other octahedra with their long axes along body diagonals could indeed have been drawn.

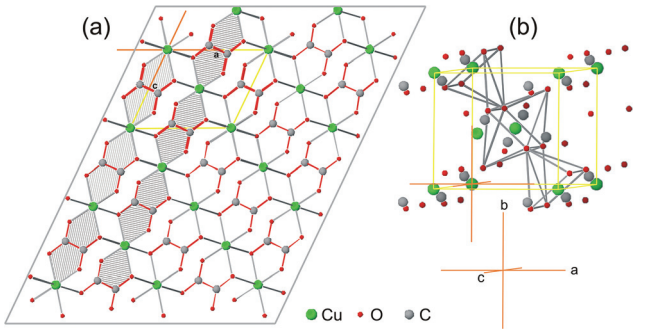

Fig. 11 (a) Displays the projection along the 010 direction of the model structure of the Cu1 CuC_2O_4 crystallite. Only bonded atoms within the grey outline box are shown. The oxalate ions are planar and tilted about 45° relative to the *ac*-plane. Four oxalate $C_2O_4^{2-}$ ions centred at the yellow unit cell borders are indicated by thick red bonds. The remaining oxalate ions are shown by thin red bonds. Two planar CuC_2O_4Cu tilted bands are indicated by the grey hatched pentagons along the ***c***-axis in (a). The bands are tilted approximately 45° from the *ac*-plane. The copper ion has a planar coordination to four oxygen atoms with two Cu1–O1 = 1.890(10) Å bond distances (grey) and two Cu1–O2 = 2.066(8) Å (grey) that are coordinated to two oxygen atoms with Cu1–O2 = 2.483(9) Å bond distances (black) perpendicular to the coordination plane. The coordination is forming deformed oxygen octahedra. As examples, (b) shows one full octahedron and two half octahedra. The bond lengths differ slightly for the two octahedra and other octahedra with their long axes along other body diagonals could have been drawn.

The magnetic properties of CuC_2O_4 are quite interesting and intriguing. Clear evidence for well isolated one-dimensional chains of Cu^{2+} bridged by oxygen has been found. They are similar to chain structures found in honeycomb lattices like $Na_3Cu_2SbO_6$,[21–23] and Cu_5SbO_6,[24] and the one-dimensional spin chain compound $LiCuSbO_4$.[25] Like CuC_2O_4 they all have characteristic nearest-neighbour Cu–O bond lengths in the range of 1.9 to 2.0 Å and show no magnetic ordering down to low temperatures (for $LiCuSbO_4$ down to 100 mK). While the magnetic properties of these compounds are well accounted for by the use of one-dimensional Cu^{2+}-spin chain models the CuC_2O_4 behaviour is more subtle. The energy gap

derived from the Bleaney–Bowers fit to the susceptibility is quite high, Δ = 442 K. As already mentioned, the fact that the Bleaney–Bowers model accounts quite nicely for high temperature susceptibility is not a proof of isolated Cu^{2+}–Cu^{2+} dimers in CuC_2O_4. The copper–oxygen chain structure derived in this work does not support the formation of such isolated dimers and quite similar susceptibilities may result from linear chain models with competing interactions. Furthermore, the low concentration of dimers established by the Bleaney–Bowers fit indicates that this model is inappropriate. Very accurate susceptibility measurements are required in this context, but are difficult to obtain because of the large paramagnetic background that may have a weak temperature variation. Eventually, the large background may result directly from the linear chain excitations. Similar large constant paramagnetic contributions have been found in earlier studies and appear to be intrinsic.[20] Neutron scattering measurements of the excitation spectrum combined with detailed model work would be quite valuable to resolve this question. Thus, CuC_2O_4 is an interesting compound that may add new aspects to our understanding of one-dimensional frustrated magnetic systems.

Appendix: profile parameters used for the X-rays and neutron diffraction patterns

For most diffraction patterns the continuous resolution function derived by FullProf in the profile matching mode will adequately describes the peak shape in the full 2θ-range of the patterns. During the course of this investigation, it became obvious that independent of the sample and the type of radiation, the instrument resolution parameters deduced by the FullProf matching of the peak profiles in the patterns (Fig. 1–4) failed to describe the variation of the observed broad

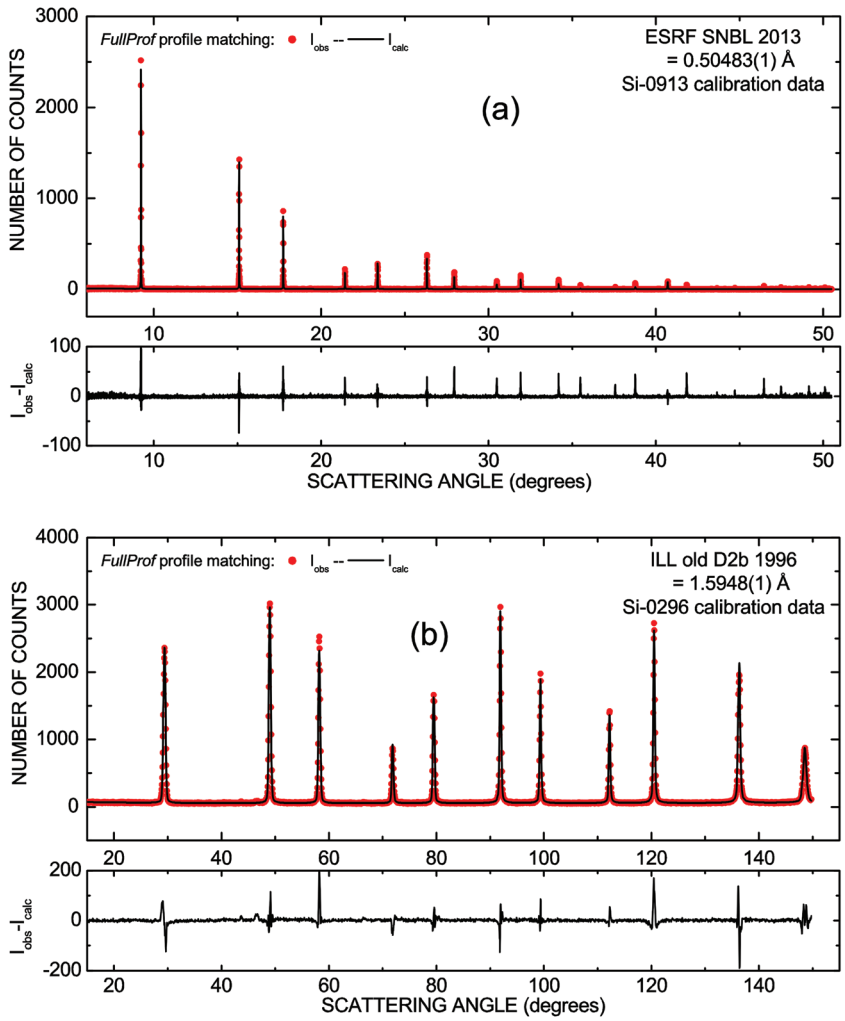

Fig. 12 Powder synchrotron X-ray diffraction pattern (a) of Si-0913 (λ = 0.50483(1) Å) and (b) neutron diffraction pattern of Si-0296 (λ = 1.5949(1) Å). The upper panels in (a) and (b) show the observed (●) and calculated patterns (black curves) and the lower panels show the corresponding difference plots. The profile-matching mode (Le Bail) was applied in the program FullProf using a = 5.431021 Å ($Fd\bar{3}m$) in order to calibrate the wavelength and determine the profile parameters listed with normal characters in columns 4 and 5 of Table 3, respectively.

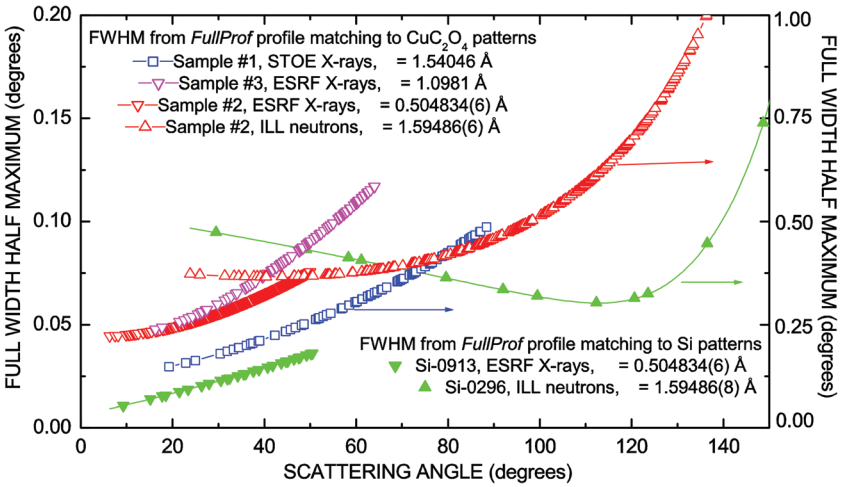

Fig. 13 Full width at half maximum *versus* scattering angles determined by profile matching of the CuC_2O_4 peaks (Fig. 1–4) and the Si peaks in the instrument calibration diffraction patterns (Fig. 12(a) and 12(b)). It should be noted that the results for the STOE X-ray data (Fig. 1) and the ILL neutron data (Fig. 4) are displayed *versus* the right hand ordinate. The profile parameters for the curves with open red, blue and magenta signatures are listed by italics in columns 2 to 5 of Table 3. The profile parameters for the green curves with filled triangles are listed by normal characters in columns 4 and 5 of Table 3.

and narrow peaks. Nevertheless, these profile parameters were adequate for use in test refinements of different structural models. These structural models were the original orthorhombic Schmittler[9,10] model and the monoclinic model for β-ZnC_2O_4.[11] When combined with the results from the *ab initio* FOX calculation in section 4.3, the latter model led to the idea of the randomly stacked monoclinic model proposed in the present work in section 4.4.

The first attempt at structural refinement of the randomly stacked model was done using the neutron data in Fig. 4 (sample 2) and FullProf with pseudo Voigt peaks described by *U*, *V*, *W* from ref. 27 with refined *Y* (Table 3, column 4, italics). This attempt was promising, and subsequent inclusion of the size and strain effects as described in section 4.5 modelled the peak width variation reasonably well. Using the structural parameters *x*, *y*, *z* found by refinement of the neutron result with the synchrotron X-ray pattern in Fig. 2 (sample 3) in conjunction with the sample dependent profile parameters (Table 3, column 2, italics) was disappointing, and the inclusion of the size and strain effects failed completely. Obviously better instrument profile parameters were needed. With help from colleagues at ILL (A. C. Hewat and E. Suard) an instrument Si calibration data set (Si-0296 collected at the same time as the neutron data of sample 2) was provided. Recently, W. van Beek at ESRF supplied an additional synchrotron data set of CuC_2O (Fig. 3, sample 2) and the corresponding instrument Si calibration data set Si-0913. The cooperation of these colleagues is highly appreciated.

The present appendix contains the Si-0913 and Si-0296 synchrotron X-ray (Fig. 12a) and neutron (Fig. 12b) diffraction data, respectively. The profile matching of these data was done using pseudo Voigt peaks (Npr = 7), which is a prerequisite of FullProf when including the size and strain effects. The resulting profile parameters for the Si instrument calibration data and the CuC_2O sample/instrument profile parameters are summarised in Table 3 and referred to throughout section 4. A summary plot of profile widths (FWHM) *versus* scattering is shown in Fig. 13 for all parameter sets listed in Table 3. For completeness, Table 4 contains the parameters used for the contour plots of size and strain distributions shown in Fig. 10 and described in section 4.5.

Table 4 Size and strain parameters used for the contour plots of the size and strain distributions shown in Fig. 10

Neutron diffraction data					
Profile parameters listed in italics in column 5 in Table 3					
Anisotropic size parameters for Laue class 2/*m* (size-model = 15)					
Y00	3.54	*Y20*	1.37	*Y22+*	−1.93
Y22−	−0.22	*Y40*	1.64	*Y42+*	−0.44
Y42−	2.55	*Y44+*	0.48	*Y44−*	0.24
Anisotropic strain parameters for Laue class 2/*m* (strain-model = 2)					
S_400	31.2	*S_040*	17.1	*S_004*	1.50
S_220	37.9	*S_202*	50.9	*S_022*	−0.79
S_121	24.2	*S_301*	63.7	*S_103*	16.3
Synchrotron X-ray diffraction data					
Profile parameters listed in normal characters in column 4 in Table 3					
Anisotropic size parameters for Laue class 2/*m* (size-model = 15)					
Y00	5.54	*Y20*	0.96	*Y22+*	−3.60
Y22−	3.31	*Y40*	6.59	*Y42+*	3.58
Y42−	−3.26	*Y44+*	0.10	*Y44−*	−1.44
Anisotropic strain parameters for Laue class 2/*m* (strain-model = 2)					
S_400	9.55	*S_040*	4.52	*S_004*	0.49
S_220	−0.11	*S_202*	12.29	*S_022*	−2.59
S_121	−11.25	*S_301*	17.55	*S_103*	3.87

Acknowledgements

The following institutions are acknowledged for the use of their experimental facilities: National Synchrotron Light

Source, Brookhaven National Laboratory, Upton, NY, USA, European Synchrotron Radiation Facility, Grenoble, France and Institute Max von Laue–Paul Langevin, Grenoble, France. We gratefully acknowledge the following colleagues for valuable cooperation during this work: Jonathan C. Hanson, Torben René Jensen, Poul Norby, Helmer Fjellvåg, Wouter van Beek, Alan C. Hewat and Emmanuelle Suard. The copper(II) oxalate sample 3 was kindly provided by Helmer Fjellvåg.

References

1 T. Echigo, M. Kimata, A. Kyono, M. Shimizu and T. Hatta, *Mineral. Mag.*, 2005, **69**, 77.
2 D. A. Reed and M. M. Olmstead, *Acta Crystallogr., Sect. B: Struct. Crystallogr. Cryst. Chem.*, 1981, **37**, 938.
3 R. M. Clarke and I. R. Williams, *Mineral. Mag.*, 1986, **50**, 295.
4 J. E. Chisholm, G. C. Jones and O. W. Purvis, *Mineral. Mag.*, 1987, **51**, 715.
5 L. C. Soare, P. Bowen, J. Lemaître and H. Hofmann, *J. Phys. Chem.*, 2006, **B110**, 17763.
6 N. Jongen, H. Hofmann, P. Bowen and J. Lemaitre, *J. Mater. Sci. Lett.*, 2000, **19**, 1073.
7 D. Broadbent, J. Dollimore, D. Dollimore and T. A. Evans, *J. Chem. Soc., Faraday Trans.*, 1991, **87**, 161.
8 C. Chen, Z. Lou and Q. Chen, *Chem. Lett.*, 2005, **34**, 430.
9 H. Schmittler, *Monatsber. Dtsch. Akad. Wiss. Berlin*, 1968, **10**, 581 (JCPDS card no. 21-297).
10 H. Fichtner-Schmittler, *Cryst. Res. Technol.*, 1984, **19**, 1225.
11 Yu. Kondrashev, V. S. Bogdanov, S. N. Golubev and G. F. Pron, *J. Struct. Chem.*, 1985, **26**, 90.
12 A. Michalowicz, J. J. Girerd and J. Goulon, *Inorg. Chem.*, 1979, **18**, 3004.
13 N. Jongen, P. Bowen, J. Lemaître, J.-C. Valmalette and H. Hofmann, *J. Colloid Interface Sci.*, 2000, **226**, 189.
14 A. Boultif and D. Louër, *J. Appl. Crystallogr.*, 2004, **37**, 724.
15 J. Rodríguez-Carvajal, *Physica B*, 1993, **192**, 55.
16 A. P. Hammersley, S. O. Svensson, M. Hanfland, A. N. Fitch and D. Hausermann, *High Pressure Res.*, 1996, **14**, 235.
17 B. Donkova and D. Mehandjiv, *J. Mater. Sci.*, 2005, **40**, 388.
18 L. Dubicki, C. M. Harris, E. Kokot and R. L. Martin, *Inorg. Chem.*, 1966, **5**, 93.
19 B. N. Figgis and D. J. Martin, *Inorg. Chem.*, 1966, **5**, 100.
20 K. T. McGregor and Z. G. Soos, *Inorg. Chem.*, 1976, **15**, 2159.
21 Y. Miura, R. Hirai, Y. Kobayashi and M. Sato, *J. Phys. Soc. Jpn.*, 2006, **75**, 084707.
22 Y. Miura, Y. Yasui, T. Moyoshi, M. Sato and K. Kakurai, *J. Phys. Soc. Jpn.*, 2008, **77**, 104709.
23 M. Schmitt, O. Janson, S. Golbs, M. Schmidt, W. Schnelle, J. Richter and H. Roser, 2014, arXiv:1402.1091v1 [Cond-mat.].
24 E. Climent-Pascual, P. Norby, N. H. Andersen, P. W. Stephens, H. W. Zandbergen, J. Larsen and R. J. Cava, *Inorg. Chem.*, 2011, **51**, 557–565.
25 S. E. Dutton, M. Kumar, M. Mourigal, Z. G. Soos, J.-J. Wen, C. L. Broholm, N. H. Andersen, Q. Huang, M. Zbiri, R. Toft-Petersen and R. J. Cava, *Phys. Rev. Lett.*, 2012, **108**, 187206.
26 M. G. Banks, R. K. Kremer, C. Hoch, A. Simon, B. Ouladdiaf, J.-M. Broto, H. Rakoto, C. Lee and M.-H. Whangbo, *Phys. Rev. B: Condens. Matter*, 2009, **80**, 24404.
27 A. N. Christensen and B. Lebech, *Dalton Trans.*, 2012, **41**, 1971.
28 V. Favre-Nicolin and R. Cerny, *Mater. Sci. Forum*, 2004, **443–444**, 35, (EPDIC8).
29 The neutron scattering lengths for O, D and C are 5.805, 6.67 and 6.65 F, respectively. The D–D distance in the D_2O molecule was restrained to 1.70 Å, and the C–C, and O–O distances in the oxalate ion are close to 1.57 and 2.17 Å, respectively.
30 R. L. Frost, K. Erickson and M. Weier, *J. Therm. Anal. Calorim.*, 2004, **77**, 851.
31 A. Gleizer, F. Maury and J. Galy, *Inorg. Chem.*, 1980, **19**, 2074.